Fibers and Polymers 2015, Vol.16, No.10, 2112-2120
DOI 10.1007/s12221-015-4705-3

ISSN 1229-9197 (print version)
ISSN 1875-0052 (electronic version)

Enzymatic Surface Modification of Sisal Fibers (*Agave Sisalana*) by *Penicillium echinulatum* Cellulases

Jeaneth T. Corredor González*, Aldo J. Pinheiro Dillon[1], Aly R. Pérez-Pérez[2], R. Fontana[1], and Carlos Pérez Bergmann

Department of Materials, Federal University of Rio Grande do Sul, Porto Alegre RS 90035-190, Brazil
[1]*Institute of Biotechnology, University of Caxias do Sul, Caxias do Sul RS 95070-560, Brazil*
[2]*Earth Sciences Institute, Central University of Venezuela, Caracas 1010-A, Venezuela*
(Received October 8, 2014; Revised March 14, 2015; Accepted July 16, 2015)

Abstract: We report on the effect of a new microbial enzymatic system, *Penicillium echinulatum* cellulase, on the surface morphological (SEM), structural (XRD), and thermal (TGA/DTG) properties as well as the surface chemical composition (FT-IR and FT-Raman) of sisal fibers (*Agave sisalana*)—a potential replacement for glass fibers in composite materials. Cellulase treatment greatly improved the properties of sisal fibers, rendering the surface topography and chemical composition of the fibers free of contaminants and reducing the content of amorphous materials (hemicellulose, pectin, lignin, and disordered cellulose) to yield the crystalline cellulose network. Thermal stability and crystallinity were also greatly enhanced. This work demonstrated that microbial enzymes offer an inexpensive and environmentally attractive option to improve the surfaces of natural fibers for composite applications.

Keywords: Enzymatic treatment, Microbial cellulose, *Penicillium echinulatum*, Sisal fiber, Surface properties

Introduction

Plant or vegetable fibers possess distinctive characteristics (e.g., low density, low cost, non-abrasive nature, high filling level, low energy consumption, and high strength) suitable for a variety of applications [1]. They offer a unique opportunity to explore new potential applications, mainly because of the availability of fibers with high productivity and low production cost as well as their renewable and biodegradable character. For instance, sisal fiber (*Agave sisalana*) is one of the four most widely used natural fibers in industry and accounts for almost half the total production of textile fibers due to the ease of cultivation of sisal plants with short renewal times [2]. Nearly 4.5 million tons of sisal fibers are produced annually throughout the world, and Brazil is one of the main producing countries [3].

Chemically, each fiber is esentially a complex composite of cellulose, hemicellulose, lignin, pectin, waxes, and water soluble substances. Despite the large chemical composition variability, it can be said that sisal fiber is particularly composed of 74-75.2 % cellulose, 7.6-8 % lignin, 10-13.9 % hemicelluloses by weight, and the balance is due to waxes and ash [3]. Hemicellulose is a complex mixture of different polysaccharides of relatively low molecular weight (e.g., linked polymers of glucose, mannose, xylose, etc.) that show a considerable degree of chain branching without ordered sequence [4]. It is noncovalently connected with cellulose by hydrogen bonds. Lignin is a highly complex and amorphous material that comprises phenolic polymers and both aliphatic and aromatic compunds (i.e., methoxyl, carboxyl, hydroxyl, and carbonyl groups). It is both physically and chemically connected with hemicellulose. Thus, a plant fiber may be considered to be composed of cellulose chains and hemicellulose intimately associated with lignin (i.e., a lignocellulosic material).

Cellulose is the primary structural building block of most plant surfaces. It can be characterized as a high molecular weight linear homopolymer composed of β-D-glucopyranosyl units linked together by β-(1,4)-glycosidic bonds [5]; the repeating unit is cellobiose. In woody plants, these cellulose chains aggregate into highly ordered nanostructures known as nanofibrils. Nanofibrils consist of crystalline and amorphous domains with cellulose chains parallel to the principal nanofibril axis. The crystalline domains form due to intra- and intermolecular hydrogen bonds between cellulose chains and van der Waals forces among glucose molecules. Nanofibrils are usually packed into larger units to form microfibrils which, in turn, are assembled into fibers. There are four different crystalline cellulose allomorphs: I, II, III, and IV [6]. Cellulose I is the most abundant form whose crystalline structure is a mixture of two distinct forms: celluloses I_α (triclinic) and I_β (monoclinic). The relative amounts of celluloses I_α and I_β vary with the cellulose source; being I_β form dominant in higher plants.

Physically, each fiber is made up of four parts, namely the lumen and the primary, secondary, and tertiary walls; each consisting of several layers of fibrillar structures. The fibrils have either disorderly (primary), helically (outer secondary) or parallel (inner secondary) arranged microfibril networks [7].

Despite the potential industrial applications, sisal fibers remain underutilized. At present, they are mainly used as ropes for the marine and agriculture industry. Other applications

*Corresponding author: luidra@gmail.com

include twines, cords, upholstery, padding, mat, fishing nets, fancy articles (such as purses, wall hangings, tablemats, etc.) manufacturing [2]. A new potential application of sisal fibers is as reinforcing agent in polymer-based composites [8], whose mechanical properties are influenced mainly by the quality of the fiber-matrix interfaces [9]. Thus, various fiber surface modification methods have been developed to improve its adhesion properties.

Enzymatic modification of cellulose and cellulosic (or lignocellulosic) materials is an attractive, environmentally friendly, and efficient alternative to conventional physical and chemical methods. These biological treatments offer several advantages because of high reaction specificity of enzymes, milder reaction conditions, and nondestructive transformations induced on relevant surfaces [10].

Microbial (or fungal) cellulases are among the most widely used enzymes in the processing of plant fibers [11]. In general, a cellulase complex (or simply, cellulase) is a crude mixture of at least three different types of enzymes: endoglucanase, exoglucanase (cellobiohydrolase and glucocellulase), and β-glucosidase (cellobiase). They act synergistically and exhibit different activity on celluloses. Endoglucanase randomly hydrolyzes the linkages within the water-insoluble cellulose chain (i.e., cellodextrins and amorphous cellulose regions), producing oligosaccharides of various lengths and new reducing and non-reducing ends on the cellulose chains. These ends are attacked by exoglucanase, liberating glucose or cellobiose as major products. Finally, β-glucosidase converts the water-soluble cellobiose into two glucose residues.

The major drawback of the cellulase enzymatic treatments is the high cost of cellulase production [12]. Very recently, *Penicillium echinulatum* has attracted attention due to its potential to produce large amounts of cellulases at low costs [13-21].

Here, we investigated the superficial changes induced *P. echinulatum* cellulase on sisal fibers. This is part of an ongoing effort to modify the surface interfacial properties, as well as to improve the moisture resistance, of sisal fibers in cloths for fiber-reinforced composite applications. To the best of our knowledge, this is the first report that describes the enzymatic effect of *P. echinulatum* cellulases on the surface of a lignocellulosic material.

Experimental

Materials

Sisal fibers (average bundle diameter=1.4±0.3 mm and area density=960±60 g/cm^2) obtained from *Agave sisalana Perrini* plants cultivated in northeastern Brazil and made into cloth by Tecsal—Tecelagem de Sisal da Bahia, Brazil. The samples consisted of 12 cm×25 cm rectangular pieces of cloth. A sample without cellulase treatment is referred hereinafter as natural sample or fiber. The *P. echinulatum* cellulase was synthesized following the procedure described elsewhere [21].

Cellulase Treatment

The samples were treated with a cellulase concentration of 16 IU/g DM (based on the mass of oven-dry fiber, DM=dry matter) for different treatment times (t=30, 60, 90, and 120 min). Optimum enzymatic operating conditions (50 °C, pH=5.5 adjusted with a 50 mM NaOH buffer [22]) were used in a double-wall glass reactor coupled with a thermostatic bath and a mechanical stirrer operated at 175 rpm. After treatment, the samples were thoroughly washed with cold, DI water until the filtrate reached a pH~7, and then dried in ambient air.

Characterization of Fibers

Scanning Electron Microscopy (SEM)

Surface morphology was investigated by SEM using a JEOL-JSM 6060 operated at a beam current of 60 mA and an accelerating voltage of 15 kV. Since cellulose exhibits non-conducting behavior, the samples were coated prior to the analysis with a thin layer of gold by means of a plasma sputtering apparatus.

X-ray Powder Diffraction (XRD)

Room temperature XRD was performed on a powder diffractometer (X'Pert^3 powder diffractometer, PANalytical, The Netherlands) using Cu$K_{\alpha 1}$ radiation (λ=1.542 Å ; 45 kV and 35 mA). The diffractometer was used in reflection mode with a fixed angle of incidence to the sample's normal. Data were collected in the 2θ-range 5-50 ° at a step size of 0.010 ° with 6 s exposure at each step. Dried samples were manually cut into small pieces to make a finely ground powder. Approximately 100 mg of powder was dispersed and held between two tightly pressed glass substrates for analysis.

Prior to analysis, the profiles were normalized by the area under the intensity-angle curve. Numerical integration by the trapezoidal rule was performed using IGOR Pro (a trademark of WaveMetrics, Inc.) scientific data analysis software. The normalized XRD patterns were then resolved into individual peaks and a constant background using a curve fitting procedure with Gaussian functions:

$$I(2\theta) = I_0 + \sum_{i=1}^{n} I_i \exp\left[-\frac{\pi(2\theta - 2\theta_i)^2}{\beta_i^2}\right] \quad (1)$$

where 2θ is the diffraction angle, n the number of peaks, I_i the peak height (or maximum intensity), and β_i the integral breadth of the peak located at $2\theta=2\theta_i$. The integrated intensity or peak area of a Gaussian component is $A_i=I_i\beta_i$. The nonlinear least-squares curve fitting was carried out using the Levenberg-Marquardt algorithm and the multi-peak fitting package implemented in the IGOR Pro software.

The degree of crystallinity (i.e., the weight fraction of the crystalline portion) of the samples was evaluated from the normalized and deconvoluted XRD patterns using the crystallinity index CI equation below [23]:

$$CI = \left(\frac{A_c}{A_c + kA_a}\right) \times 100\% \quad (2)$$

where A_c (A_a) is the integrated intensity of the crystalline (amorphous) peaks, and k (=1 for the sake of simplicity) is an empirical constant dependent on the nature, density, and mass absorption coefficient of both crystalline and amorphous components.

The apparent crystallite size $D_\perp$ and the lattice spacing d were estimated from the (200) lattice plane using the Scherrer [24] and Bragg equations, respectively:

$$D_\perp \approx \frac{0.89 \cdot \lambda}{\beta \cos\theta} \quad (3)$$

$$\lambda = 2d\sin\theta \quad (4)$$

Thermogravimetric Analysis (TGA)

TGA was performed on a TGA analyzer (TGA/SDTA 851e, Mettle-Toledo). Small amounts of samples (~7-10 mg) were used in order prevent heat and mass transfer limitations. The experiments were carried out under a N_2 atmosphere at a flow rate of 40 ml/min. The samples were heated in the range from T=30 °C to 900 °C at a constant heating rate of 10 °C/min. DTG curves (w' versus T) were obtained by central-difference numerical differentiation of the TGA curves (w versus T). We deconvoluted and fitted the DTG curves using logistic distribution functions:

$$w'(T) = w_0' + \sum_{i=1}^{n} w_i' \mathrm{sech}^2\left(\frac{2T - 2T_i}{\beta_i}\right) \quad (5)$$

where w_i' is the peak amplitude or maximum weight loss rate, and T_i is the peak position or decomposition temperature T_m.

Fourier Transform Infrared Spectroscopy (FT-IR)

FT-IR spectroscopy measurements were performed at room temperature using a mid-IR spectrophotometer (IRAffinity-1S FT-IR spectrometer, Shimadzu Corporation), equipped with a DLaTGS pyroelectric detector and a single reflection ATR accessory. A minimum of 21 scans was run in the wavenumber region of 600-3200 cm^{-1}, with a spectral resolution of 1 cm^{-1}. Each sample was measured three times.

Fourier Transform Raman Spectroscopy (FT-Raman)

Raman spectra were acquired with a microscope-spectrometer system (inVia Reflex, Renishaw plc), equipped with a 785 nm diode laser for excitation (maximum output power of 100 mW), a CCD array detector, and a high-resolution microscope (DM2500M, Leica Microsystems). Data were collected in a 180 backscattering geometry and the laser beam was focused on the fiber using a 50× magnification objective. A minimum of 21 accumulations was acquired in the spectral range of 1600-500 cm^{-1}, with a 0.85 cm^{-1} resolution and 1 s exposure at each step. Each sample was measured three times using different sampling areas.

Results and Discussion

Morphological Analysis by SEM

Figure 1 shows SEM micrographs of the sisal samples before and after cellulase treatment. The surface of the

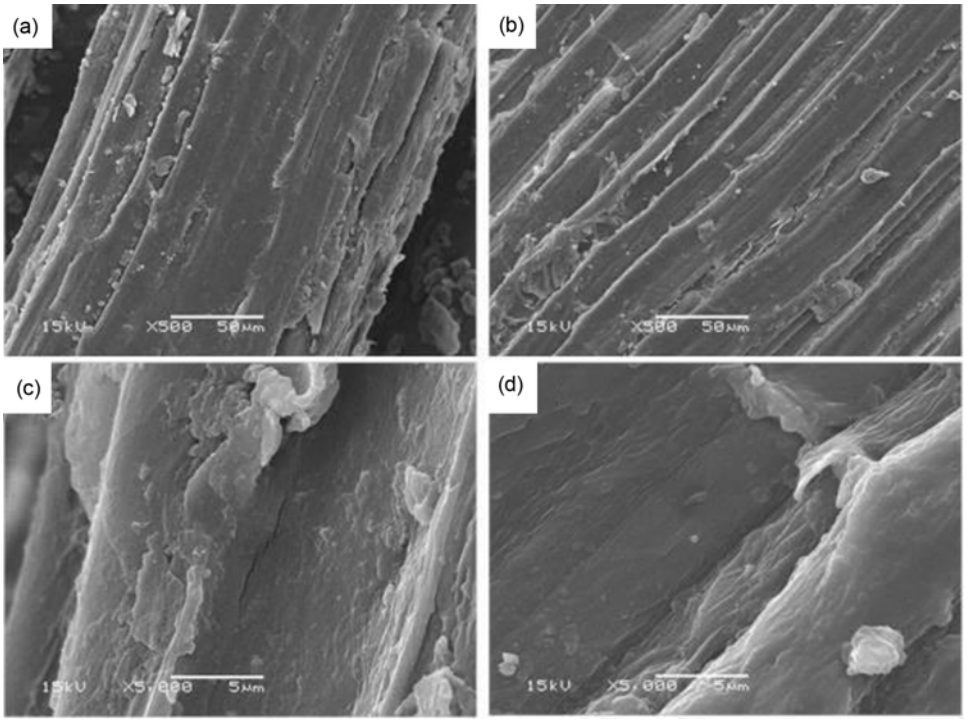

Figure 1. SEM micrographs for the (a, c) natural and (b, d) cellulase-treated sisal sample (t=120 min).

natural sample was covered with a thin layer, unevenly distributed along the fiber surface (Figure 1(a)). This layer consists mainly of intercellular binding materials in addition to amorphous waxy cuticle [25]. The removal of this layer during cellulase treatment increased the surface roughness revealing the morphology of the fiber bundles (Figure 1(b)). The surfaces are marked, in both cases, by their characteristic vestigial attachments of the parenchymatous cells in which the fiber was embedded in the leaf. Cellulase treatment leads to the partial removal of these fragments and bundles of individual cell elements can be seen on the surface of the clean sample. The individual fiber cells are discontinuous and consist of short length units joined end to end by lignin-rich, weak intermolecular bonds. Moreover, the cellulase treatment withdraws several layers of cells, revealing some internal structures of the fibers.

Figure 1(c) and Figure 1(d) show higher resolution SEM micrographs of the same samples. Cellulase gradually attacks the fiber to remove amorphous hemicellulose and lignin materials from its surface and expose its inner layers, resulting in fibers cleaner than natural ones.

A recent study conducted on bamboo fibers using a number of enzymes (xylanase, cellulase, pectin lyase, and laccase) revealed that the different enzymatic systems were effective in improving fiber fineness, presumably as a result of the removal of the more polar hemicellulosic fraction [26]. More recently, flax and hemp fibers were treated with different enzymatic systems (xylanase, xylanase + cellulase, polygalacturonase, laccase, pectinmethylesterase); each treatment rendered the surface topography of both fibers free of contaminants and yielded the individual fiber bundles [27]. Depending on the chemistry of the coupling agent, it is expected that this cleaner surface of the fibers result in better bonding during composite manufacturing [28].

Structural Properties by XRD

Figure 2 shows typical XRD profiles for all the samples before data normalization. The natural sample had similar spectrum to the cellulase-treated ones, but the later had slightly higher intensity (with a few exceptions), so the crystallinity and crystallite size of cellulose must have been improved and affected by the cellulase treatment. Comparison of the XRD spectrum of the untreated sample and that of each cellulase-treated sample reveals that the ordered structure of the crystalline region of the fibers did not undergo any polymorphic transformation during the enzyme treatment. However, the peak positions were observed to shift slightly toward lower 2θ values as t increased. This may be the result of the progressive rearrangements of the cellulose crystal lattice.

All the XRD patterns are similar to those of typical native cellulose I_β and exhibit very distinct features; mainly the presence of three broad peaks, with different integral widths and heights, superimposed on a much broader background.

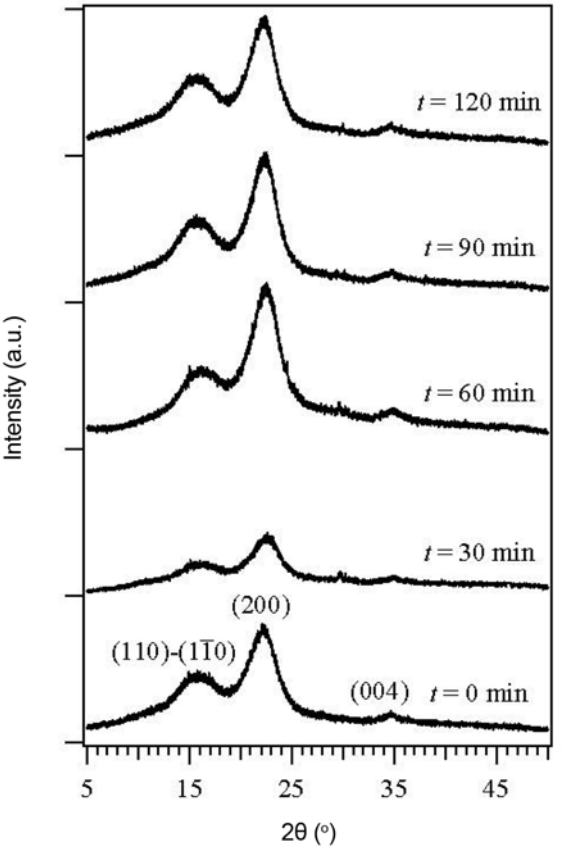

Figure 2. XRD profile of the natural and cellulase-treated samples as a function of hydrolysis time (t=0 for no treatment) on the corresponding curve. The peaks are labeled to indicate their crystal lattice assignments, assuming that the I_β phase is aligned with the fiber axis along the b direction. Three main peaks superimposed on a broad background are clearly identified; they correspond to the reflections from the (004), (200), and (1$\bar{1}$0)-(110) lattice planes.

The first peak located at 2θ=15.9±0.2° corresponds to the convolution of (1$\bar{1}$0)-(110) peaks [29]. The (1$\bar{1}$0) and (110) peaks are smeared and appear as one broad peak when a fiber contains large amounts of amorphous material, but usually separate from each other when the amount of amorphous material decreases [30]. However, all the XRD profiles exhibited considerable overlap of these peaks. The other two peaks located at approximately 2θ=22.3±0.1° and 34.9±0.1° correspond, respectively, to the (200) and (004) crystallographic planes [31].

Figure 3 illustrates a typical example of the XRD spectral analysis by peak deconvolution. Independently of t, each XRD profile was resolved into four crystalline peaks and one amorphous peak. The convoluted (1$\bar{1}$0)-(110) peak is very symmetric and exhibits a nearly constant width of β=8.1° for all the samples, so it could not be resolved into two individual peaks. The XRD spectral analysis allowed us

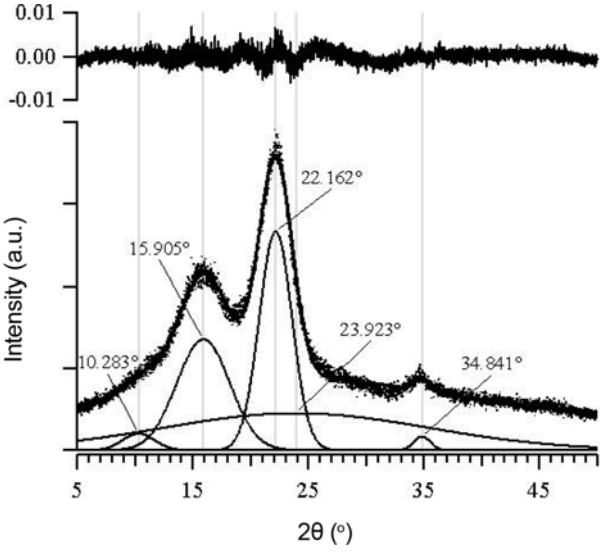

Figure 3. A typical example of the results obtained from an XRD profile normalization analysis. This spectrum corresponds to the natural sample. The solid line is the data fit to a Gaussian mixture model (equation (2)). The individual Gaussian components represent each contribution to the spectrum. The broad peak was assigned to the contributions from amorphous phases. The top inset shows the residuals, i.e., the differences between the fitted model and the data. All the spectra were fitted with a baseline $h_0=(9.0\pm0.4)\times10^{-3}$, which is close to the XRD signal of a clean glass substrate.

to identify a peak located at $2\theta=10.3\pm0.2^{\circ}$. A broad peak, at $2\theta=23.2^{\circ}$ with a constant width of $\beta=38^{\circ}$, due to the amorphous phases was also identified in all the samples.

The crystallinity indexes of our samples were calculated using equation (2). The initial CI value was $CI_0=58.4$ %, which is close to that reported for natural sisal in other studies [32,33]. During the hydrolysis, CI varied within a range of 1.5-2.0 % (Figure 4(a)). A perusal of the literature reveals that the reported changes in CI of cellulosic and lignocellulosic materials after enzymatic treatment do not show a clear behavior [34-38]. However, CI given by equation (2) proved to be sensible to crystallinity variations for our samples as a function of *t*, even within the small CI variation range (Figure 4(a)). Similar behaviors are exhibited by the crystallite size (Figure 4(b)) and lattice spacing (Figure 4(c)). This suggests that CI reflects the behavior of crystalline cellulose (i.e., crystallite packing order) rather than the proportion of this component in the sample (i.e., intrinsic crystallinity). An important assumption of equation (2) is that peak broadening is mainly caused by the increased amorphous content in the sample. However, in addition to amorphous content, other intrinsic factors (e.g., crystallite size) influence peak broadening and intensity.

CI decreased initially at $t=30$ min to start increasing monotonically with *t*, reached a maximum value, and declined again at the end of the cellulase treatment. We have attributed the initial CI decrease to the removal of surface impurities (waxy layer and oils) surrounding the fibers, swelling of the crystalline regions, and disruption of the hydrogen bonds. During cellulose swelling, the cellulase penetrates the amorphous regions located between crystallites and the cellulosic fibers and breaks the hydrogen bonds built between the macromolecules in the fiber cell wall. This leads to the destruction of the cellulose supramolecular

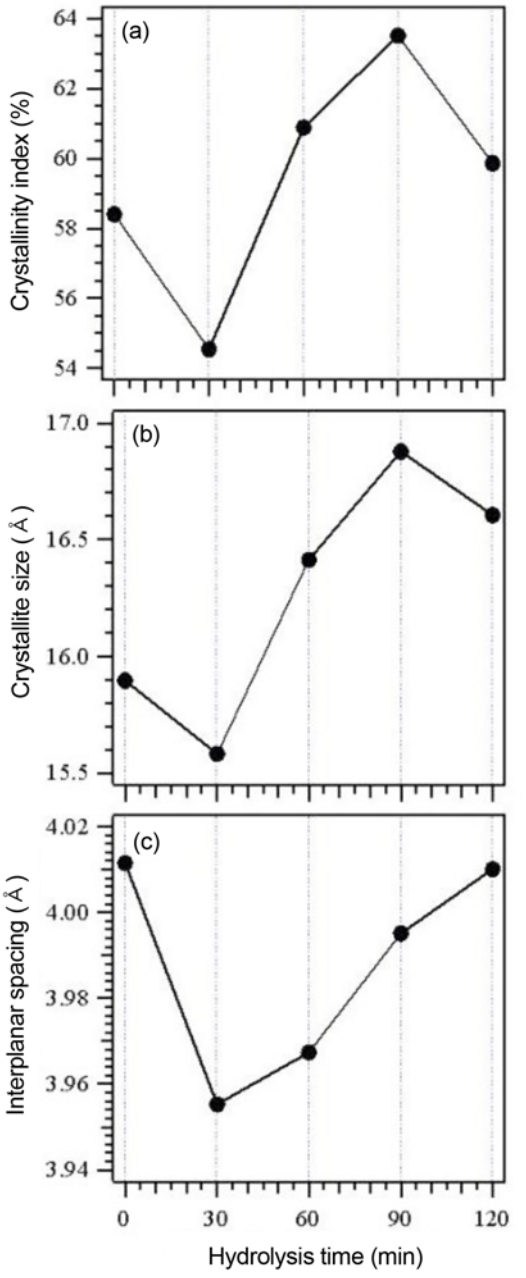

Figure 4. Time evolution of the (a) crystallinity index CI, (b) crystallite size, and (c) lattice spacing during cellulase treatment. The lines through the experimental data are guides to the eye.

structure and separation of the cellulose chains in the primary wall. Thus, swelling increases the disorder of the microfibril networks (i.e., more amorphous cellulose is generated) with the concomitant decrease of the overall CI and crystal size.

The subsequent removal of the amorphous material surrounding the cellulose microfibers results in an increase in CI. At the same time, the interfibrilar regions are likely to become less dense and less rigid and thereby make the cellulose microfibrils more capable of rearranging and packing themselves (preferably along the direction of tensile deformation). The microfibril reorganization has little effect on the chain conformation as to induce a transformation from cellulose I to cellulose II. However, better packing and stress relaxation of cellulose chains increase the crystal sizes (i.e., an increase of ~9 % and ~2 % in $D_{\perp}$ and d, respectively). When fibers stretch, such rearrangements amongst the microfibrils may result in better load sharing by them, and hence higher stress development in the fiber.

At longer-term cellulase treatment, both hydrolysis and degradation reactions affect on the cellulose regions altering the fine structure and morphology of the fibers. Hydrolysis is faster for large crystalline regions leading to a slight decrease in the overall CI and crystal sizes.

Both *Humicola insolens* cellulases and *Aspergillus* endoglucanase were found to have pronounced effect on the crystallinity and apparent crystallite size of cellulosic materials during hydrolysis, inducing increases of about 3-10 % in CI and 3-30 % in $D_{\perp}$ [36].

Thermal Properties by TGA

Figure 5 shows the results of TGA for untreated and cellulase-treated samples. Table 1 shows the thermo-analytical data as determined from the curve fitting of the spectra using equation (5). The weight loss on dry basis was calculated from each thermogram excluding the weight loss below 120 °C. Four main stages of weight loss can be distinguished during thermal decomposition of fibers:

(i) The slight weight loss (~2-3 %) in the low T region below 120 °C (T_m=64±4 °C) is due to evaporation of moisture in the fibers.

(ii) The weight loss (13 % for cellulase-treated samples and higher for natural sisal) in the T range 180-320 °C is attributed mainly to the degradation of NCP. Decomposition of lignin also takes place but in a lesser extent because of its low proportion. The average T_m~291±2 °C (onset of thermal degradation) is close to that of hemicellulose decomposition [33].

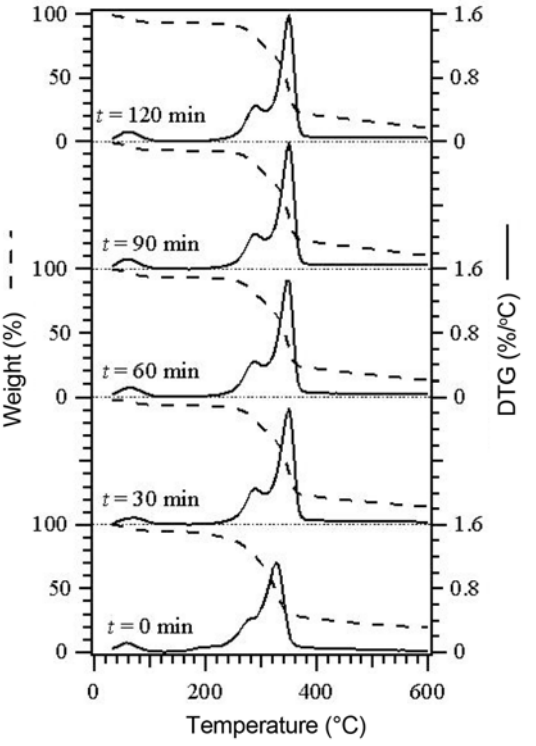

Figure 5. TG/DTG thermograms of the natural and cellulase-treated sample as a function of the hydrolysis time.

(iii) The weight loss (~8 % for natural fibers and ~10 % for cellulase-treated fibers) in the T range 320-380 °C corresponds almost exclusively to the degradation of cellulose by breaking of glycosidic linkages of the glucose chain. Pyrolysis of lignin also continues although to a much lower extent. The average T_m=348±1 °C (maximum degradation) is slightly higher than that of pure cellulose [33].

(iv) The last stage starts at 400 °C. A sustained weight loss was observed, which corresponds to the process of carbonization.

In addition to the stages observed in all the thermograms, a DTG peak located at T=203 °C and a corresponding weight loss of 9 % can be clearly identified in the thermogram of natural fiber. This weight loss may be due to the removal of the waxy layer covering the fibers.

Table 1. Thermoanalytical data TG/DTG of natural and cellulase-treated sisal samples as determined from curve fitting of the thermograms

t (min)	T_{m1} (°C)	%wt	T_{m2} (°C)	%wt	T_{m3} (°C)	%wt	T_{m4} (°C)	%wt
0	60.1	2.0	291.1	16.8	329.0	8.3	453.8	66.2
30	71.0	2.6	290.0	13.1	348.2	10.0	460.0	76.9
60	65.7	2.7	290.0	13.1	346.9	9.7	460.0	77.1
90	62.5	2.5	290.0	13.2	349.0	9.5	460.0	77.3
120	62.9	2.5	295.0	13.4	349.1	9.2	460.0	77.4

The effect of cellulase treatment (with respect to natural sisal) on the thermal decomposition of fiber (see Table 1) can be summarized as follows:

(a) Disappearance of the peak located at T=203 °C in the thermogram of natural fiber (stage ii).

(b) Increased onset of thermal degradation temperature (T_{m2}~4 °C higher, stage ii).

(c) Increased maximum degradation temperature (T_{m3}~16 °C higher, stage iii).

(d) Slightly delayed combustion stage (T_{m4}~6 °C higher, stage iv).

(e) Slightly lower weight loss due to NCP decomposition (~4 % lower, stage ii).

(f) Slightly higher weight loss due to cellulose decomposition (~2 % higher, stage iii) and combustion (~11 % higher, stage iv).

Most of the aforementioned effects result from cellulose enrichment because of the removal of substances from the cell walls. The overall result is an increased thermal stability of sisal. The cellulase treatment mostly extracts non-cellulosic components of low T_m, while the higher stability components remain in the fiber, thus increasing T_m values for the decomposition and combustion of cellulose. In addition, removal of certain amorphous material would promote better reorganization and packing of the cellulose crystallite in the fibers, hence T_m increases. On the other hand, an increase of cellulose thermal stability could also be attributed to the removal of mineral matter naturally present in minute amounts, which could promote its degradation [39,40].

Flax fibers treated with xylanase were also characterized by higher onset of degradation (T_{m2}~2 °C higher) and maximum degradation (T_{m3}~4 °C higher) temperatures compared to control samples, which was attributed to the removal of the least stable hemicellulosic fraction of the fibers [27]. In contrast, fibers treated with lacasse exhibited the opposite behavior (i.e., T_{m2}~2 °C and T_{m3}~2 °C lower). Laccase is responsible for removing the lignin fraction of the fibers, thereby exposing the less stable hemicellulose and cellulose, which correlated to a decrease in these properties because the structure is less rigid [27].

Surface Chemical Composition by FT-IR and FT-Raman

The IR spectra of cellulose, hemicellulose, and lignin have been previously reported in the literature [41-43]. These materials are mainly composed of alkanes, esters, aromatics, ketones, and alcohols, with different oxygen-containing functional groups. Figure 6 shows the FT-IR spectra of both natural and cellulase-treated samples. FT-IR spectrum for natural fibers shows the following functional groups:

(a) The C-OH bending peak is observed between 610-668 cm^{-1}.

(b) The C-C stretching at 1029 cm^{-1} and the C-H asymmetric out of phase ring stretching of cellulose at 896 cm^{-1} were also detected and related to the β-glucosidic linkages between the glucose units in hemicellulose and cellulose.

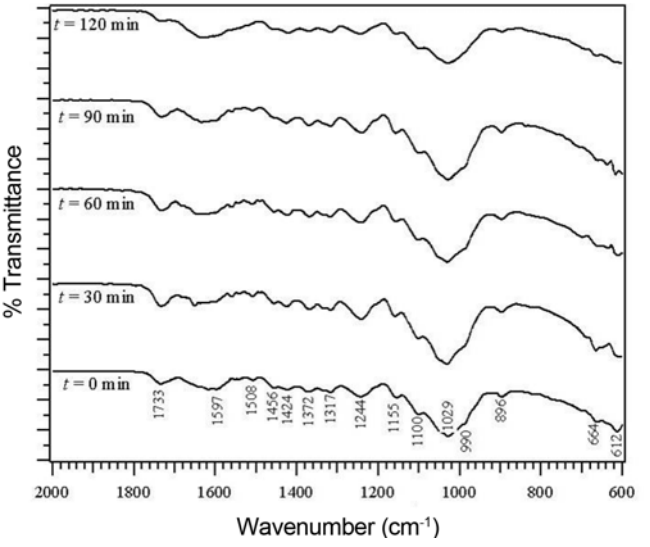

Figure 6. FT-IR spectrum of the natural and cellulase-treated samples as a function of the hydrolysis time.

(c) The peak at 1100 cm^{-1} resulted from C-OH groups in cellulose, hemicellulose, and lignin.

(d) The peak at 1244 cm^{-1} represents the C-O stretching of the acetyl groups of cellulose and lignin. It could also be attributed to the C-H bending of lignin and hemicellulose.

(e) The 1317 cm^{-1} and 1155 cm^{-1} wave numbers are attributed to the CH_2 wagging and C-O-C asymmetric bridge stretching of cellulose, respectively.

(f) The peak at 1424 cm^{-1} is due to the CH_2 symmetric bending of hemicellulose.

(g) Lignin and fatty oils presented characteristic peaks in the range 1450-1600 cm^{-1} (1456, 1508, and 1597 cm^{-1}) corresponding to the aromatic skeletal vibration. The peak at 1597 cm^{-1} is due to C=C stretching.

(h) The band at 1733 cm^{-1} appears in all of the spectra. It could be attributed to the C=O stretching of the acetyl groups of cellulose, hemicelluloses, and pectin [44]. On the other hand, it could be a carboxylic or aldehyde absorption arising from the open terminal glycopyranose rings or oxidation of the C-OH groups [42].

With cellulase treatment, a decrease in the intensity of some peaks respect to natural fibers was observed. Thus, the band located at 1244 cm^{-1} region associated with the C-O ring of lignin diminished, and the band at 1733 cm^{-1} related with carboxylic groups present in pectins and hemicellulose almost disappeared. The slight increase of this peak intensity at the earliest stages of cellulase treatment probably occurred from degradation of the cellulose and the subsequent opening of a glucose unit to generate a carboxyl functional group. A decrease in the intensity of this band was observed upon cellulase treatment of fibers for 120 min due to removal of

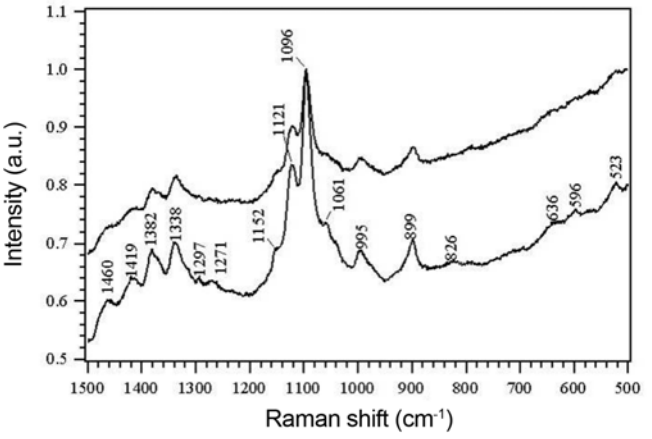

Figure 7. FT-Raman spectrum of the (a) natural and (b) cellulase-treated sisal sample (t=120 min).

hemicelluloses from the fiber surface. Other important changes are related with the reduction of peak intensities between 3200-3600 cm^{-1} (not shown) that correspond to the reduction of some hydroxyl groups associated with the vibration modes of chemical substances as carbohydrates [45] and fatty acids present in the fibers [46].

Figure 7 shows the FT-Raman spectra of natural and cellulase-treated samples. The Raman lines at 1121 and 1096 cm^{-1}, assigned to the skeletal C-O-C vibrational modes of the β-(1,4)-glycosidic linkages of the β-D-glucopyranosyl units of cellulose, can serve as characteristic marker bands for such multicomponent systems like cellulosic plant tissues. The intensity of these two Raman lines decreased upon cellulase treatment. The intensity of the peak at 995 (rotating), 1338, 1392, 1419, and 1460 cm^{-1} (bending) due to CH_2 vibrational modes of cellulose also decreased. The peak at 1460 cm^{-1}, which is greatly reduced upon cellulase treatment, is a typical CH_2 bending vibration of amorphous cellulose [47]. The CH_2 twisting bands at 1271 and 1297 cm^{-1} disappeared upon cellulase treatment.

Conclusion

A recently developed microbial cellulase derived from *Penicillium echinulatum* was utilized to modify the surface of fibers in an aqueous medium. Different analytical techniques were employed to examine the effect of surface treatment, including SEM, XRD, FT-IR spectroscopy, and TGA/DTG. These analyses revealed that cellulase treatment resulted in better fiber properties concerning to composite fabrication. In particular, TGA/DTG studies showed enhanced thermal stability in treated fibers due to removal of waxy substances and lignin from the cell walls. The treatments caused exposure of the cellulose structures in cleaner surfaces, as observed by SEM. The results of X-ray diffraction revealed that fiber with and without cellulase treatment exhibits the same crystalline lattice of cellulose I, with well resolved ($1\bar{1}0$)-(110), (200), and (004) reflections. An unassigned peak was identified at about 10 when the XRD spectra were deconvoluted using Gaussian functions. The very similar behaviors exhibited by the crystallinity index and lattice dimensions indicated that fiber crystallinity improved due to partial removal of amorphous components, which results in the adjustment in the cellulose molecular structure. FT-IR and FT-Raman spectra of both natural and cellulase-treated sisal samples looked almost the same except for the slightly diminished intensity of some characteristic peaks due to the removal of hemicellulose-, pectin-, and lignin-like components upon cellulase treatment. These results indicate that the surface properties of fiber can be tailored to facilitate the interface of composites, and enzymatic treatment using a cellulase derived from *Penicillium echinulatum* can be a potential alternative to traditional chemical treatments or pretreatments to modify cellulose fibers.

References

1. S. K. Batra in “Handbook of Fiber Chemistry”, 3rd ed. (M. Lewin Ed.), pp.454-505, CRC Press, Boca Raton, 2006.
2. P. S. Mukherjee and K. G. Satyanarayana, *J. Mater. Sci.*, **19**, 3925 (1984).
3. K. G. Satyanarayana, J. L. Guimarães, and F. Wypych, *Compos. Pt. A-Appl. Sci. Manuf.*, **38**, 1694 (2007).
4. R. H. Atalla, J. W. Brady, J. F. Matthews, S.-Y. Ding, and M. E. Himmel, “Biomass Recalcitrance: Deconstructing the Plant Cell Wall for Bioenergy” (M. E. Himmel Ed.), pp.188-212, Blackwell Publishing Ltd., Oxford, 2008.
5. D. Klemm, B. Philipp, T. T. Heinze, U. Heinze, and W. Wagenknecht, “Comprehensive Cellulose Chemistry: Fundamentals and Analytical Methods”, Vol. 1, pp.9-29, Wiley-VCH, Weinheim, 1998.
6. S. Perez and D. Samain, *Adv. Carbohydr. Chem. Biochem.*, **64**, 25 (2010).
7. K. Joseph, R. D. Tolêdo Filho, B. James, S. Thomas, and L. H. Carvalho, *Res. Bros. Eng. Agric. Ambient.*, **3**, 367 (1999).
8. Y. Li, Y.-W. Mai, and L. Ye, *Compos. Sci. Technol.*, **60**, 2037 (2000).
9. S. Kaewkuk, W. Sutapun, and K. Jarukumjorn, *Adv. Mater. Res.*, **123**, 1123 (2010).
10. S. Kalia, K. Thakur, A. Celli, M. A. Kiechel, and C. L. Schauer, *J. Environ. Chem. Eng.*, **1**, 97 (2013).
11. M. Karmakar and R. R. Ray, *Res. J. Microbiol.*, **6**, 41 (2011).
12. D. J. Gregg, A. Boussaid, and J. N. Saddler, *Bioresour. Technol.*, **63**, 7 (1998).
13. A. J. P. Dillon, S. O. Paesi-Toresan, and L. P. Barp, *Rev. Brasil. Genet.*, **15**, 491 (1992).
14. M. Camassola, L. R. De Bittencourt, N. T. Shenem, J.

Andreaus, and A. J. P. Dillon, *Biocatal. Biotransform.*, **22**, 391 (2004).
15. N. T. Sehnem, L. R. de Bittencourt, M. Camassola, and A. J. P. Dillon, *Appl. Microbiol. Biotechnol.*, **72**, 163 (2006).
16. A. J. P. Dillon, C. Zorgi, M. Camassola, and J. A. P. Henriques, *Appl. Microbiol. Biotechnol.*, **70**, 740 (2006).
17. M. Camassola and A. J. P. Dillon, *J. Appl. Microbiol.*, **102**, 478 (2007).
18. L. F. Martins, D. Kolling, M. Camassola, A. J. P. Dillon, and L. P. Ramos, *Bioresour. Technol.*, **99**, 1417 (2008).
19. M. Camassola and A. J. P. Dillon, *Ind. Crops Prod.*, **29**, 642 (2009).
20. M. Camassola and A. J. P. Dillon, *Appl. Biochem. Biotechnol.*, **162**, 1889 (2010).
21. A. J. P. Dillon, M. Bettio, F. G. Pozzan, T. Andrighetti, and M. Camassola, *J. Appl. Microbiol.*, **111**, 48 (2011).
22. M. R. Rubini, A. J. P. Dillon, C. M. Kyaw, F. P. Faria, M. J. Poças-Fonseca, and I. Silva-Pereira, *J. Appl. Microbiol.*, **108**, 1187 (2010).
23. F. H. Chung and R. W. Scott, *J. Appl. Crystallogr.*, **6**, 225 (1973).
24. J. Langford and A. J. C. Wilson, *J. Appl. Crystallogr.*, **11**, 102 (1978).
25. T. Lindström, *Colloid. Polym. Sci.*, **258**, 168 (1980).
26. L. Liu, L. Cheng, L. Huang, and J. Yu, *Fiber. Polym.*, **13**, 600 (2012).
27. M. George, P. G. Mussone, and D. C. Bressler, *Ind. Crops Prod.*, **53**, 365 (2014).
28. K. L. Pickering, G. W. Beckermann, S. N. Alam, and N. J. Foreman, *Compos. Pt. A-Appl. Sci. Manuf.*, **38**, 461 (2007).
29. Y. Liu and H. Hu, *Fiber. Polym.*, **9**, 735 (2008).
30. J. Perel, *J. Text. Inst.*, **81**, 241 (1990).
31. A. E. Oudiani, Y. Chaabouni, S. Msahli, and F. Sakli, *Carbohydr. Polym.*, **86**, 1221 (2011).
32. D. Saikia, *Int. J. Thermophys.*, **29**, 2215 (2008).
33. M. Benítez-Guerrero, J. López-Beceiro, P. E. Sánchez-Jiménez, and J. Pascual-Cosp, *Thermochim. Acta*, **581**, 70 (2014).
34. S. D. Mansfield, E. de Jong, R. S. Stephens, and J. N. Saddler, *J. Biotechnol.*, **57**, 205 (1997).
35. G. Buschle-Diller, C. Fanter, and F. Loth, *Text. Res. J.*, **69**, 244 (1999).
36. Y. Cao and H. Tan, *Enzyme Microb. Technol.*, **36**, 314 (2005).
37. L. Wang, Y. Zhang, P. Gao, D. Shi, H. Liu, and H. Gao, *Biotechnol. Bioeng.*, **93**, 443 (2006).
38. Y. Chen, A. J. Stipanovic, W. T. Winter, D. B. Wilson, and Y.-J. Kim, *Cellulose*, **14**, 283 (2007).
39. G. Várhegyi, M. J. Antal, E. Jakab, and P. Szab, *J. Anal. Appl. Pyrolysis*, **42**, 73 (1997).
40. D. Vamvuka, S. Troulinos, and E. Kastanaki, *Fuel*, **85**, 1763 (2006).
41. S. Y. Oh, D. I. Yoo, Y. Shin, and G. Seo, *Carbohydr. Res.*, **340**, 417 (2005).
42. V. A. Alvarez and A. Vazquez, *Compos. Pt. A-Appl. Sci. Manuf.*, **37**, 1672 (2006).
43. H. Yang, R. Yan, H. Chen, D. H. Lee, and C. Zheng, *Fuel*, **86**, 1781 (2007).
44. P. Ganan, S. Garbizu, R. Llano-Ponte, and I. Mondragon, *Polym. Compos.*, **26**, 121 (2005).
45. K. K. Pandey, *J. Appl. Polym. Sci.*, **71**, 1969 (1999).
46. L. Y. Mwaikambo and M. P. Ansell, *J. Appl. Polym. Sci.*, **84**, 2222 (2002).
47. K. Schenzel and S. Fischer, *Lenzinger Berichte*, **83**, 64 (2004).